Electronic Supplementary Material (ESI) for Journal of Materials Chemistry C.

Overcoming the luminescence instability of colloidal mixed-halide perovskite quantum dots through ion motion confinement

Xinli Wang, [a] *Yang Sun,*[a] *Jie Gao,*[a] *Xiao Huang,*[a] *Dandan Cao,*[a] *Xiaowen Gao,*[b] *Hao-Yi Wang,*[a] *Qi Li,*[b] *Yi Wang**[a] *Li-Min Fu,*[a] *Xi-Cheng Ai,*[a] *Dongsheng Xu,*[b] *Jian-Ping Zhang**[a]

[a]Key Laboratory of Advanced Light Conversion Materials and Biophotonics, Department of Chemistry, Renmin University of China, Beijing, 100872, China

[b]Beijing National Laboratory for Molecular Sciences, State Key Laboratory for Structural Chemistry of Unstable and Stable Species, College of Chemistry and Molecular Engineering, Peking University, Beijing, 100871, China

AUTHOR INFORMATION

Corresponding Authors：

*Yi Wang, E-mail: ywang@ruc.edu.cn

*Jian-Ping Zhang, E-mail: jpzhang@ruc.edu.cn

Contents

S1. Size distribution histograms of $CsPbBr_{1.5}I_{1.5}$ QDs

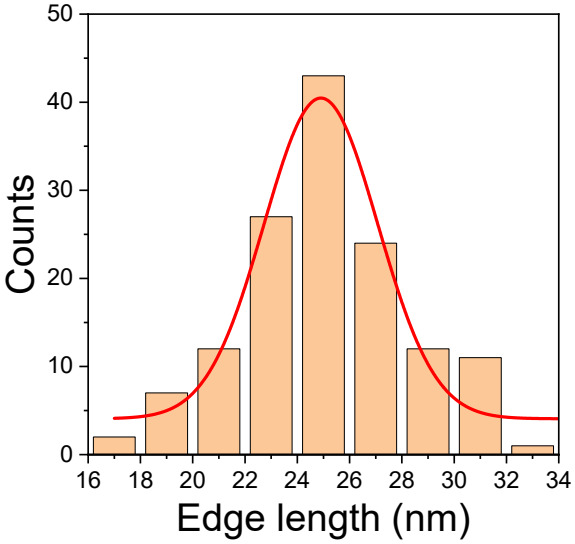

Fig. S1. Size distribution histogram of the $CsPbBr_{1.5}I_{1.5}$ QDs. The red curve shows the fitting result of the Gaussian distribution function, which yields an average edge length of ~ 25 ± 3 nm for the cube-like nanocrystals.

S2. In-situ, real-time PL spectra of $CsPbBr_3$ QDs at different temperatures

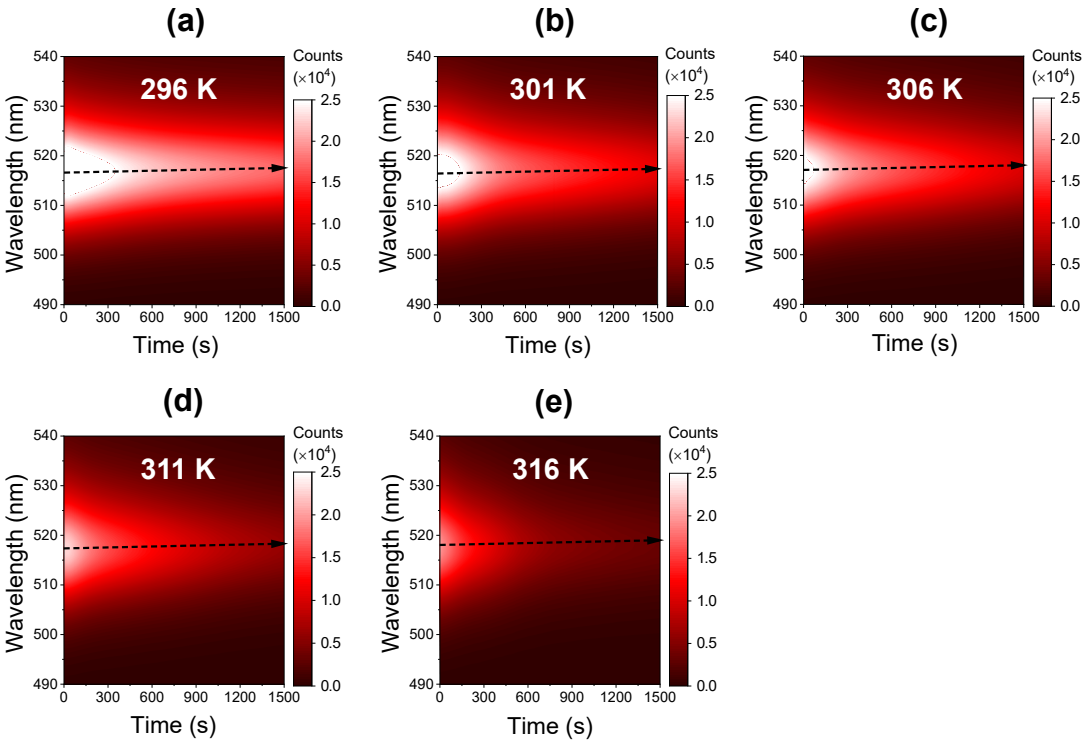

Fig. S2. Temporal evolution of the PL spectra of $CsPbBr_3$ QDs illuminated by a CW laser at different temperatures. (a) 296 K, (b) 301 K, (c) 306 K, (d) 311 K and (e) 316 K.

Compared with the mixed halide PQDs, $CsPbBr_3$ QDs are more photostable owing to the absence of the light-driven migration of iodide ions. Even so, the intensity of PL still declines upon the long-term CW illumination, because of the ligand desorption that leads to nanocrystal aggregation in the context of interparticle van der Waals attraction forces.[1, 2] In addition, it is noted that the initial PL intensity is reduced with increasing the temperature as attributed to the thermal quenching effect of the trap states.[3, 4] Also observed is a slight redshift of the PL wavelength, as ascribed to the physical aggregation of the nanocrystals that reduces the quantum confinement effect.[5] The redshift value is only ~0.6 nm, which is likely due to the large size of as-synthesized $CsPbBr_3$ QDs where the dependence of bandgap on the particle size is relatively weak.

S3. Dependence of the PL wavelength of $CsPbBr_3$ QDs on temperature

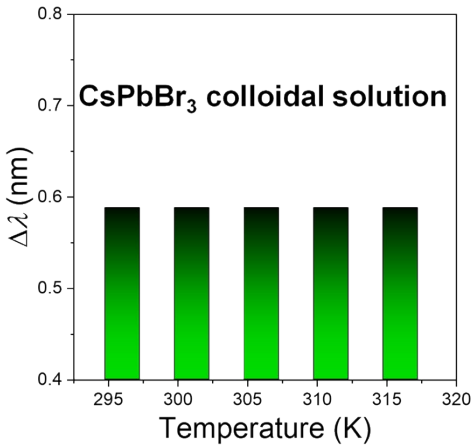

Fig. S3. The value of wavelength redshift for $CsPbBr_3$ QDs illuminated by a CW laser for 25 min at different temperatures, which are calculated from the in-situ, real-time PL spectra presented in Fig. S2.

S4. PL spectra evolution of $CsPbBr_{1.5}I_{1.5}$ QDs at different temperatures

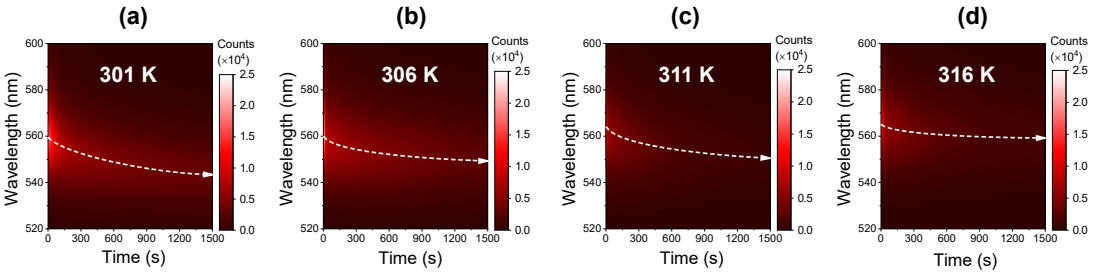

Fig. S4. Temporal evolution of the PL spectra of $CsPbBr_{1.5}I_{1.5}$ QDs illuminated by a CW laser at different temperatures. (a) 301 K, (b) 306 K, (c) 311 K and (d) 316 K.

The temperature-dependent PL spectra evolution for $CsPbBr_{1.5}I_{1.5}$ QDs upon the long-term CW illumination is depicted in Fig. S4. In addition to the decrease of PL intensity, the wavelength blueshifts significantly, which is distinctly different from the case for $CsPbBr_3$ QDs (Fig. S2). This helps us to exclude the possibility of assigning the PL instability of $CsPbBr_{1.5}I_{1.5}$ QDs to the aforementioned effect of nanocrystal aggregation.

S5. Temperature-dependent PL wavelength change of $CsPbBr_{1.5}I_{1.5}$ QDs

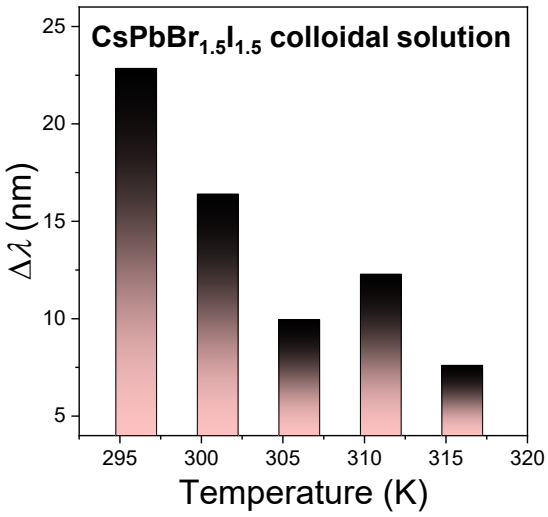

Fig. S5. The value of wavelength blueshift for $CsPbBr_{1.5}I_{1.5}$ QDs illuminated by a CW laser for 25 min at different temperatures, which are calculated from the in-situ, real-time PL spectra presented in Fig. S4.

S6. Diagram of the thermodynamics of the ion migration equilibrium

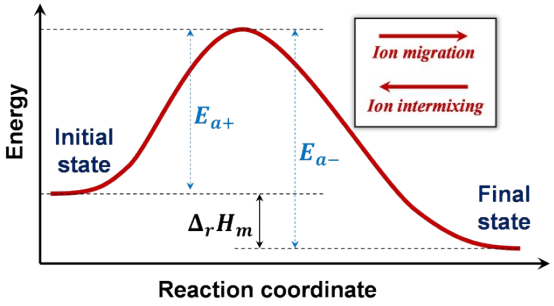

Fig. S6. Energy profile of the ion migration reaction derived from the temperature-dependent temporal evolution of PL spectra for $CsPbBr_{1.5}I_{1.5}$ QDs (Fig. S5) based on the second law of thermodynamics (see text for details).

Note S1: The evolution of PL spectra as a function of temperature (Fig. S4 and Fig. S5) provides deeper insights into the mechanism of ion migration and ion intermixing. For simplicity, we use the subscripts "+" and "–" to represent the ion migration reaction and the ion intermixing reaction, respectively. Because ion intermixing is a spontaneous process without the need for optical excitation, according to the second law of thermodynamics, it must obey the following inequation:

$$\Delta_r G_{m,-} = \Delta_r H_{m,-} - T\Delta_r S_{m,-} < 0 \qquad (Eq.\ S1)$$

where T, $\Delta_r G_{m,-}$, $\Delta_r H_{m,-}$, and $\Delta_r S_{m,-}$ denote the experimental temperature, Gibbs free energy change, enthalpy change, and entropy change reaction, respectively, for the ion intermixing.

In addition, considering the reaction equilibrium between ion migration and ion intermixing, the thermodynamics parameters can be linked with the equilibrium constant (K) via the van't Hoff equation:

$$lnK_{+/-} = -\frac{\Delta_r H_{m,+/-}}{RT} + \frac{\Delta_r S_{m,+/-}}{R} \qquad (Eq.\ S2)$$

where R is the universal gas constant.

Fig. S4 and Fig. S5 show that the ion migration-induced wavelength blueshift is suppressed (*i.e.*, decrease in K_+) with increasing the experimental temperature, indicative of a negative (positive) value of $\Delta_r H_{m,+}$ ($\Delta_r H_{m,-}$) based on Eq. S2. In other words, the initial state of the ion migration reaction possesses a higher potential energy than the final state, as schematically illustrated in Fig. S6. Also derived from the energy profile is that the activation energy of ion migration is less than ion intermixing (*i.e.*, $E_{a+} < E_{a-}$), which is in excellent agreement with the experimental results that ion migration is much more rapid than ion intermixing. Meanwhile, according to Eq. S1, $\Delta_r H_{m,-}$ should be less than $T\Delta_r S_{m,-}$ to ensure a negative $\Delta_r G_{m,-}$ value, whereby one can further get the inequation, $T\Delta_r S_{m,-} > \Delta_r H_{m,-} > 0$. This implies that the ion intermixing in the dark is an entropy-driven process, and the light-driven ion migration accompanies entropy reduction.

S7. PL spectra evolution of $CsPbBr_{1.5}I_{1.5}$ QDs treated with different amounts of OA/OAm

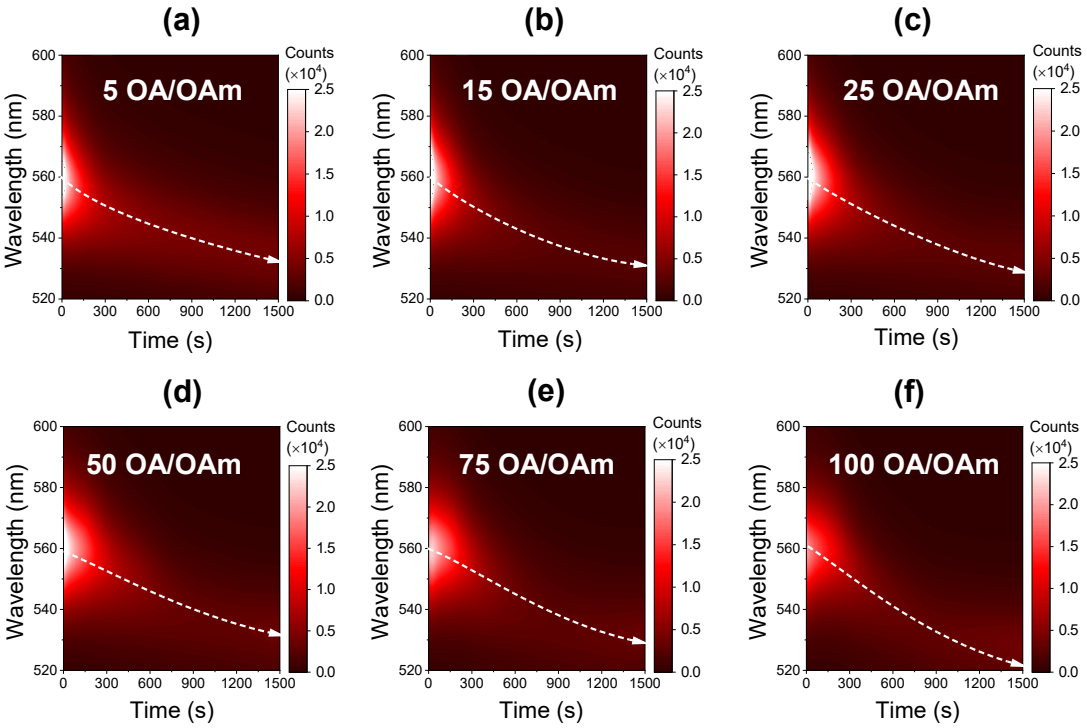

Fig. S7. Temporal evolution of the PL spectra of $CsPbBr_{1.5}I_{1.5}$ QDs treated with different amounts of OA/OAm under the illumination of the CW laser. From panel (a) to panel (f), the amount of OA/OAm is successively increased (see text for details).

For the OA/OAm post-treatment, x μL of OA and x μL of OAm were first added to 1 mL of toluene to prepare the OA/OAm solution, where x = 5, 15, 25, 50, 75, or 100 as denoted in the different panels of Fig. S7. Then, 3 μL of the purified $CsPbBr_{1.5}I_{1.5}$ QDs and 2 μL of the OA/OAm solution were mixed in 600 μL of toluene following sufficient stirring. Compared with the untreated sample shown in Fig. 1c, the initial PL intensity is dramatically increased upon the OA/OAm post-treatment, implying the enhancement of PLQY. However, with the prolongation of the illumination time, both

the decline of PL intensity and the blueshift of PL wavelength become more severe. This suggests that the OA/OAm post-treatment is in favor of improving the short-term PL performance but exacerbates the PL instability of the $CsPbBr_{1.5}I_{1.5}$ QDs solution.

S8. PL spectra evolution of $CsPbBr_{1.5}I_{1.5}$ QDs treated with different amounts of SBE

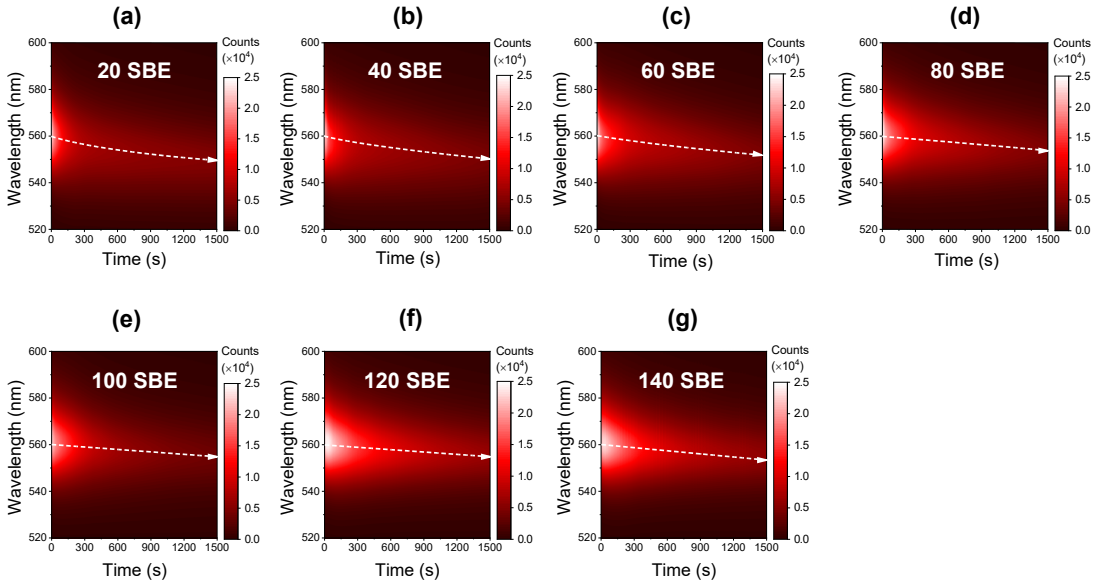

Fig. S8. Temporal evolution of the PL spectra of $CsPbBr_{1.5}I_{1.5}$ QDs treated with different amounts of SBE under the illumination of the CW laser. From panel (a) to panel (f), the amount of SBE is successively increased (see text for details).

For the SBE post-treatment, 2 mg of SBE was first added to 10 mL of toluene and then thoroughly stirred until the complete dissolution of SBE. Then, 3 μL of the purified $CsPbBr_{1.5}I_{1.5}$ QDs and y μL of the SBE solution were mixed in toluene with a desired volume to ensure the mixed solution is 600 μL, where y = 20, 40, 60, 80, 100, 120, or 140 as denoted in the different panels of Fig. S8. Compared with the untreated sample shown in Fig. 1c, the initial PL intensity is only slightly increased, while the light-induced PL blueshift is suppressed with the increase of SBE amount, which indicates that SBE can improve the PL stability but does not remarkably elevate the PLQY.

S9. Absolute PLQY spectra of samples with different ligands

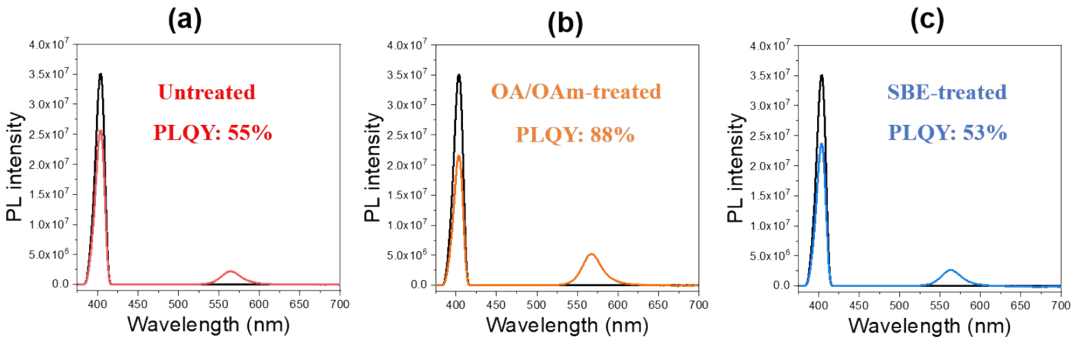

Fig. S9. The absolute PLQY spectra of $CsPbBr_{1.5}I_{1.5}$ QDs (a) without ligand post-treatment, (b) post-treated with OA/OAm, and (c) post-treated with SBE, respectively.

S10. PL spectra evolution of $CsPbBr_{1.5}I_{1.5}$ QDs treated with different amounts of SBE/OA/OAm

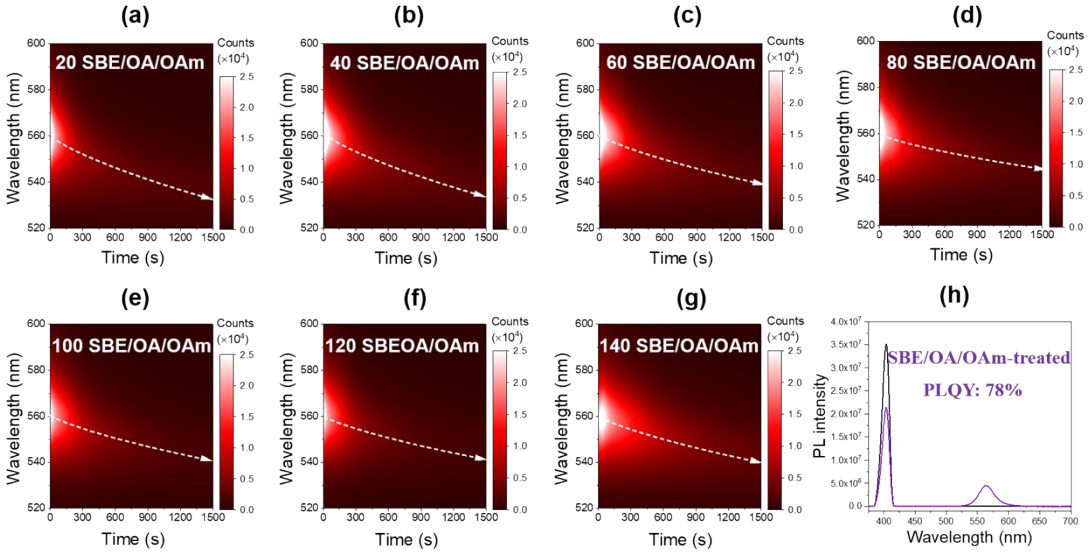

Fig. S10. Temporal evolution of the PL spectra of $CsPbBr_{1.5}I_{1.5}$ QDs treated with different amounts of SBE/OA/OAm under the illumination of the CW laser. From panel (a) to panel (g), the amount of SBE/OA/OAm is successively increased (see text for details). (h) The absolute PLQY spectra of 80 SBE/OA/OAm.

For the SBE/OA/OAm post-treatment, we first prepare the OA/OAm solution with an x value of 15 (see details in S8) and the SBE solution by dissolving 2 mg of SBE in 10 mL of toluene. Then, 3 μL of the purified $CsPbBr_{1.5}I_{1.5}$ QDs, 2 μL of the OA/OAm solution, and z μL of the SBE solution were mixed in toluene with a desired volume to ensure the mixed solution is 600 μL, where z = 20, 40, 60, 80, 100, 120, or 140 as denoted in the different panels of Fig. S10. Compared with the untreated sample shown in Fig. 1c, both the PLQY and the PL stability are ameliorated. Closer inspection concerning the compromise between the PLQY and the PL stability shows that the optimal sample is achieved when the value of z is 80, which corresponds to the tested sample shown in the manuscript.

S11. HRTEM images of $CsPbBr_{1.5}I_{1.5}$ QDs

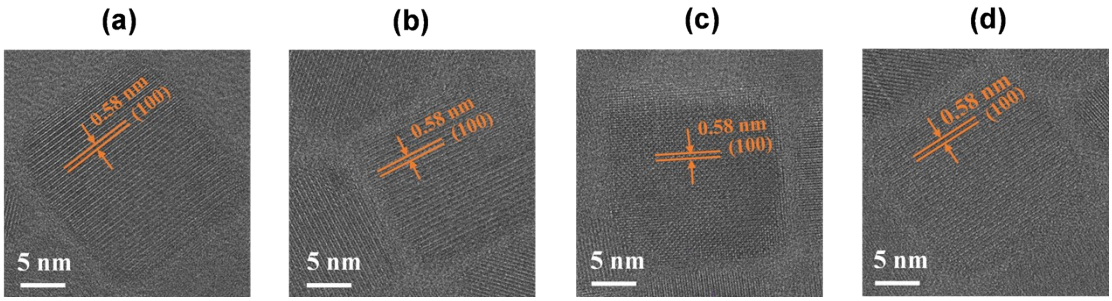

Fig. S11. HRTEM images of $CsPbBr_{1.5}I_{1.5}$ QDs (a) without ligand post-treatment, (b) post-treated with OA/OAm, (c) post-treated with SBE, and (d) post-treated with SBE/OA/OAm, respectively.

S12. XRD patterns of $CsPbBr_{1.5}I_{1.5}$ QDs

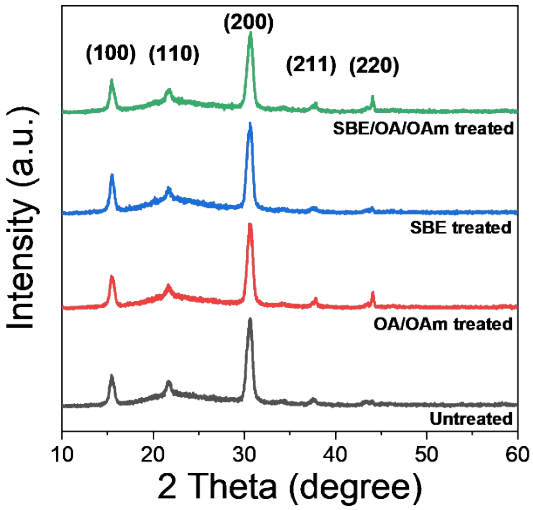

Fig. S12. XRD patterns of $CsPbBr_{1.5}I_{1.5}$ QDs without ligand post-treatment (black), post-treated with OA/OAm (red), post-treated with SBE (blue), and post-treated with SBE/OA/OAm (green), respectively.

All the tested samples show the same characteristic refraction peaks at 15°, 22°, 31°, 38°, and 42°, which are assigned to the (100), (110), (200), (211), and (220) lattice planes of the cubic phase for the mixed-halide PQDs, respectively.[6] This indicates that the used ligand post-treatment methods do not influence the nanocrystalline structure of $CsPbBr_{1.5}I_{1.5}$ QDs.

S13. FTIR spectra of $CsPbBr_{1.5}I_{1.5}$ QDs

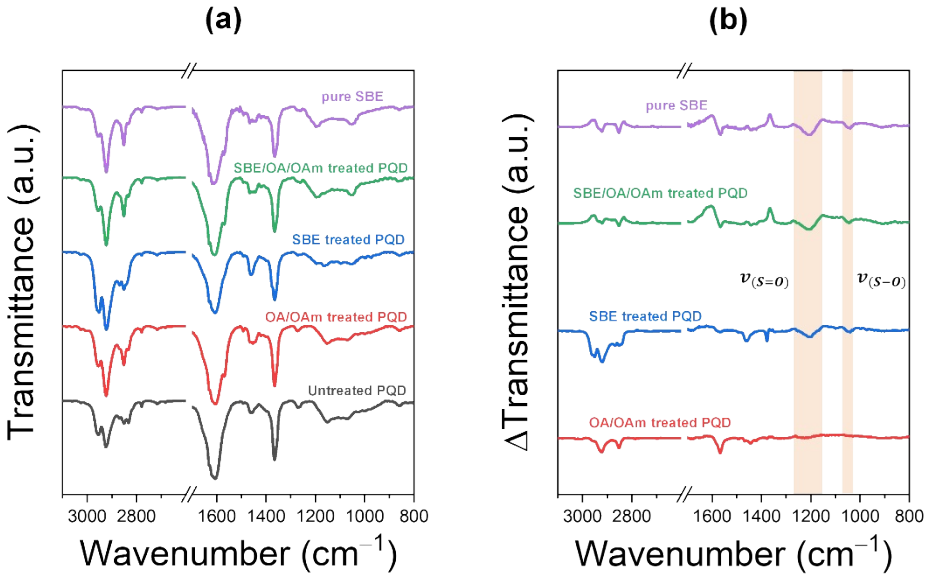

Fig. S13. (a) FTIR spectra of $CsPbBr_{1.5}I_{1.5}$ QDs without ligand post-treatment (black), post-treated with OA/OAm (red), SBE (blue), and SBE/OA/OAm (green), as well as the pure SBE ligand (purple), respectively. (b) Corresponding difference transmittance FTIR spectral (see text for details).

To evaluate the interaction between the SBE ligand and the surface of PQDs, FTIR spectra of the PQDs without or with the post-treatment and of the pure organic ligands were measured, as displayed in Fig. S13(a). By normalizing the transmission signals at ~3050 cm^{-1} to unity and then subtracting the spectrum of the untreated PQDs from the others, we get the corresponding FTIR difference spectra (Fig. S13(b)). Characteristic FTIR peaks at ~1200 cm^{-1} and ~1050 cm^{-1}, as attributed to the stretching vibration of the S=O bond and S–O bond respectively,[7] are unambiguously seen for pure SBE, SBE-treated, and SBE/OA/OAm-treated PQDs while absent for OA/OAm-treated PQDs. This indicates that SBE has been successfully attached to the surface of $CsPbBr_{1.5}I_{1.5}$ nanocrystals.

S14. High-solution XPS spectra of $CsPbBr_{1.5}I_{1.5}$ QDs

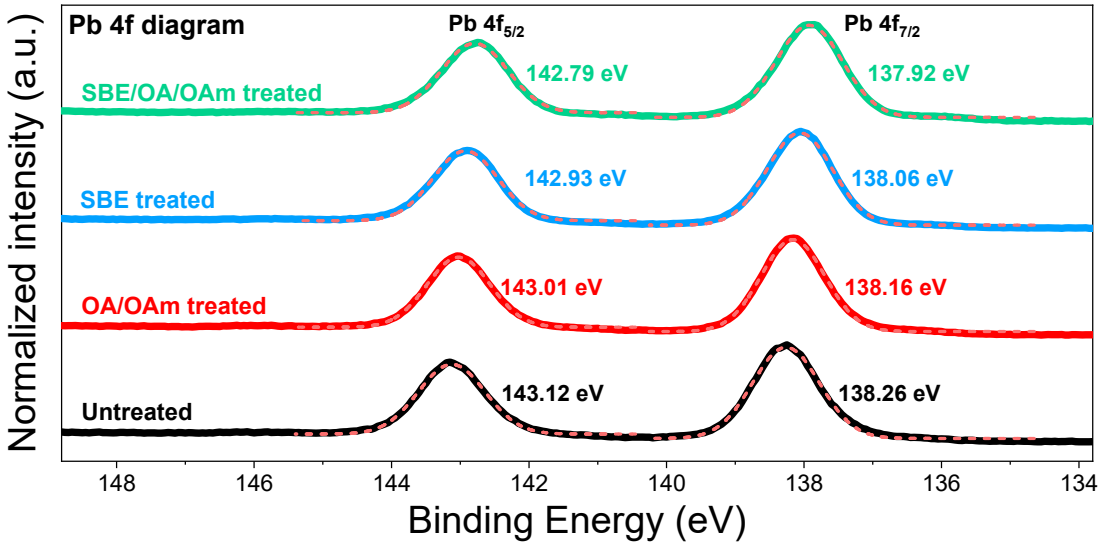

Fig. S14. High-resolution XPS spectra (Pb 4f diagram) of $CsPbBr_{1.5}I_{1.5}$ QDs without ligand post-treatment (black), post-treated with OA/OAm (red), post-treated with SBE (blue), and post-treated with SBE/OA/OAm (green), respectively. Solid curves are experimental data, and dashed curves are fitting results based on the Gaussian functions.

High-resolution XPS spectra of $CsPbBr_{1.5}I_{1.5}$ with different post-synthesic treatments are shown in Fig. S13. By virtue of the ligand treatment, the characteristic peaks for Pb $4f_{5/2}$ and Pb $4f_{7/2}$ shift toward low-binding-energy side, regardless of the ligand species, because of the interaction between Pb^{2+} and the Lewis base component (e.g., oleic acid and SBE) that increase the electron cloud density around the Pb atom.[8] Moreover, the blueshift is more significant for the SBE and SBE/OA/OAm treated samples than the OA/OAm treated ones, which justify that SBE binds to Pb^{2+} more tightly than OA.

S15. Evolution of the PL wavelength for $CsPbBr_{1.5}I_{1.5}$ QDs in the dark

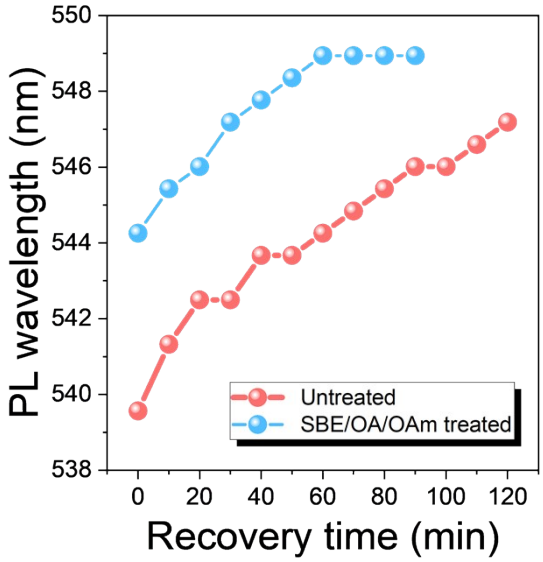

Fig. S15. Redshift of the PL wavelength as a function of recovery time for $CsPbBr_{1.5}I_{1.5}$ without (red) and with (blue) the SBE/OA/OAm post-treatment. The samples are stored in the dark following the 25-min CW excitation.

S16. Quantitative TRPL analysis of the untreated $CsPbBr_{1.5}I_{1.5}$ QDs

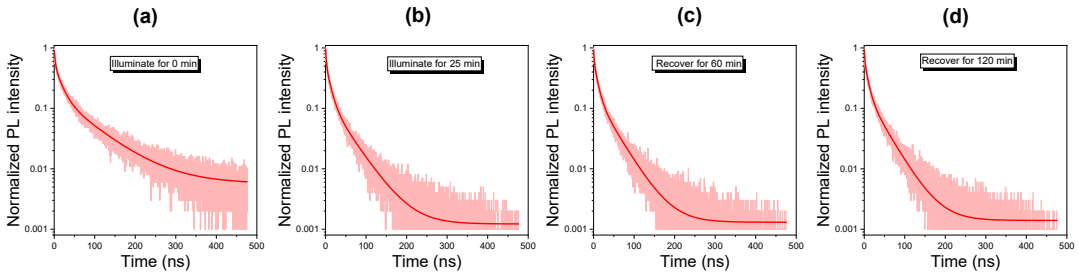

Fig. S16. TRPL kinetics of the untreated PQDs: (a) not pre-illuminated, (b) pre-illuminated for 25 min, and kept in the dark for (c) 60 min and (d) 120 min following the 25-min illumination. Red curves are experimental results, and the solid lines are fitting results based on the tri-exponential function.

Table S1. TRPL decay fitting parameters of untreated PQDs. A_i and τ_i are the pre-exponential factor and lifetime of the *i*th exponential component, and $\langle\tau\rangle$ is the average lifetime calculated according to $\langle\tau\rangle = \sum(A_i \cdot \tau_i)$.

Time	τ_1 (ns)	A_1 (%)	τ_2 (ns)	A_2 (%)	τ_3 (ns)	A_3 (%)	$\langle\tau\rangle$ (ns)
Illuminate for 0 min	2.42	40.4	15.79	42.0	79.69	17.6	21.6
Illuminate for 25 min	1.72	40.8	10.25	44.2	43.50	15.0	11.8
Recovery for 60 min	1.25	31.9	8.65	49.7	38.74	18.4	11.8
Recovery for 120 min	1.13	32.6	8.36	48.2	37.63	19.2	11.6

S17. Quantitative TRPL analysis of the SBE/OA/OAm-treated $CsPbBr_{1.5}I_{1.5}$ QDs

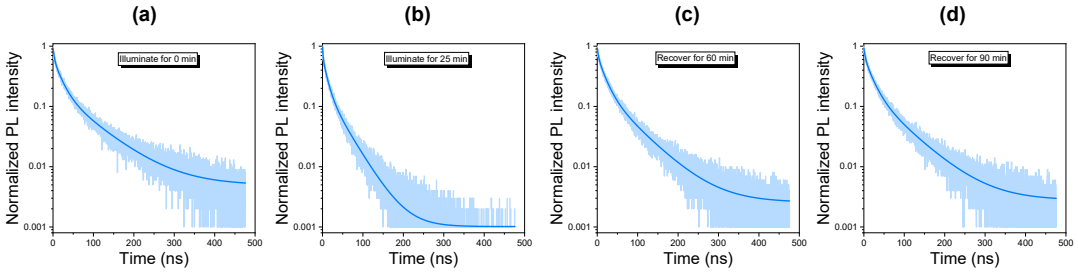

Fig. S17. TRPL kinetics of the SBE/OA/OAm-treated PQDs: (a) not pre-illuminated, (b) pre-illuminated for 25 min, and kept in the dark for (c) 60 min and (d) 90 min following the 25-min illumination. Blue curves are experimental results, and the solid lines are fitting results based on the tri-exponential function.

Table S2. TRPL decay fitting parameters of SBE/OA/OAm-treated PQDs. A_i and τ_i are the pre-exponential factor and lifetime of the *i*th exponential component, and $\langle\tau\rangle$ is the average lifetime calculated according to $\langle\tau\rangle = \sum(A_i \cdot \tau_i)$.

Time	τ_1 (ns)	A_1 (%)	τ_2 (ns)	A_2 (%)	τ_3 (ns)	A_3 (%)	$\langle\tau\rangle$ (ns)
Illuminate for 0 min	3.20	31.5	18.43	48.9	78.49	19.6	25.4
Illuminate for 25 min	1.19	32.2	10.16	47.1	38.45	20.7	13.1
Recovery for 60 min	2.80	24.9	17.32	53.6	65.04	21.5	24.0
Recovery for 90 min	3.29	27.6	18.77	51.8	69.29	20.6	24.9

S18. Evolution of the PL intensity for SBE/OA/OAm-treated $CsPbBr_{1.5}I_{1.5}$ QDs

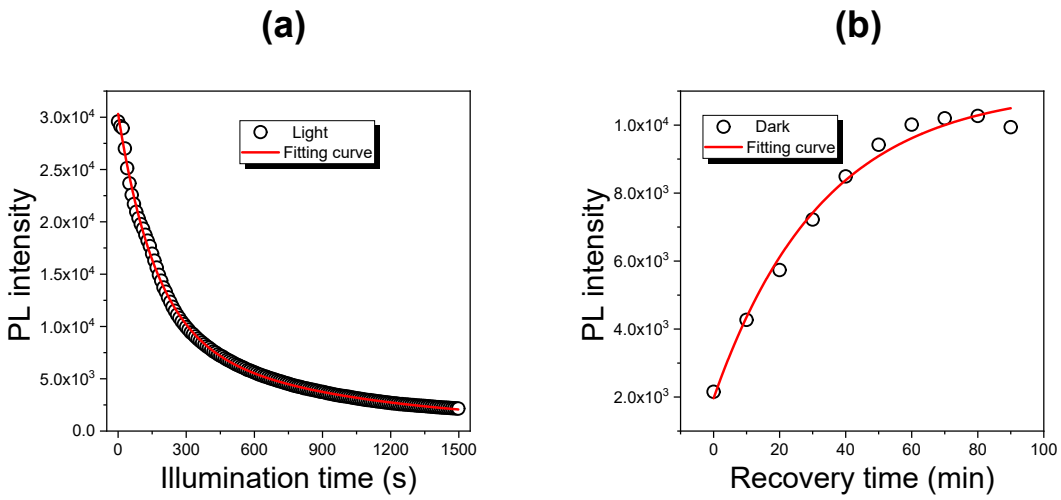

Fig. S18. PL intensity of SBE/OA/OAm-treated PQDs as a function of (a) illumination time for the sample under CW illumination and (b) recovery time for the sample stored in the dark following a 25-min CW illumination. Black circles are experimental data, and solid red curves are the exponential fitting results.

The PL intensity decay and growth kinetics are phenomenologically fitted by the exponential functions, which yield a time constant of ~370 s and ~1980 s for the former (*i.e.*, ion migration under illumination) and the latter (*i.e.*, ion intermixing in the dark), respectively. Therefore, in order to get stable PL under the PWM excitation, the value of t_{ON}/t_{OFF} (see Fig. 4a in the manuscript) is suggested to be less than 1980/370 ≈ 5.4 corresponding to a duty cycle of ~15.6%.

S19. Evolution of PL spectra for the untreated $CsPbBr_{1.5}I_{1.5}$ QDs under PWM excitation

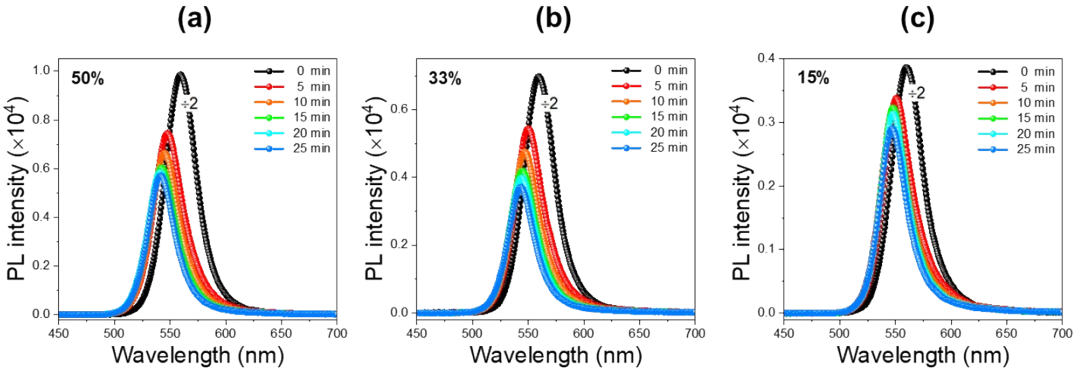

Fig. S19. PL spectra of the untreated $CsPbBr_{1.5}I_{1.5}$ QDs with different illumination times under the PWM excitation. The repetition rate is fixed at 10 kHz, and the duty cycles are (a) 50%, (b) 33%, and (c) 15%, respectively.

The light-induced PL decline and blueshift are suppressed by reducing the duty cycle, whereas they are still obvious when the duty cycle is ~15%, as attributed to the fact that the light-driven ion migration is much more rapid than the ion intermixing in the dark for the untreated $CsPbBr_{1.5}I_{1.5}$ QDs.

S20. Evolution of PL spectra for the SBE/OA/OAm-treated $CsPbBr_{1.5}I_{1.5}$ QDs under PWM excitation

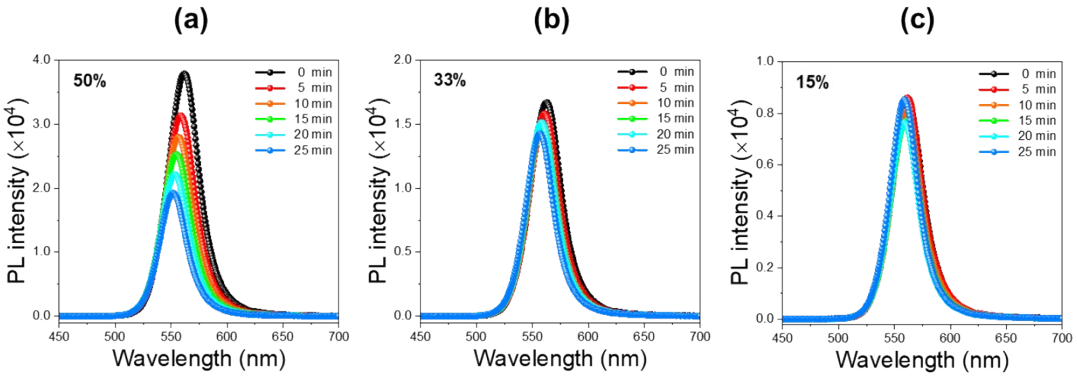

Fig. S20. PL spectra of the SBE/OA/OAm-treated $CsPbBr_{1.5}I_{1.5}$ QDs with different illumination times under the PWM excitation. The repetition rate is fixed at 10 kHz, and the duty cycles are (a) 50%, (b) 33%, and (c) 15%, respectively.

The dependence of the PL stability on the duty cycle is more remarkable for the SBE/OA/OAm-treated $CsPbBr_{1.5}I_{1.5}$ QDs. When the duty cycle is reduced to ~15%, the blueshift is only ~3 nm and the intensity decline becomes negligible. This is in excellent agreement with the results shown in Fig. S18, from which we have hypothesized that ~15% is a crucial value of the duty cycle for long-term stable PL from the SBE/OA/OAm-treated $CsPbBr_{1.5}I_{1.5}$ QDs solution.

S21. Evolution of PL spectra for the untreated $CsPbBr_{1.5}I_{1.5}$ QDs under PFM excitation

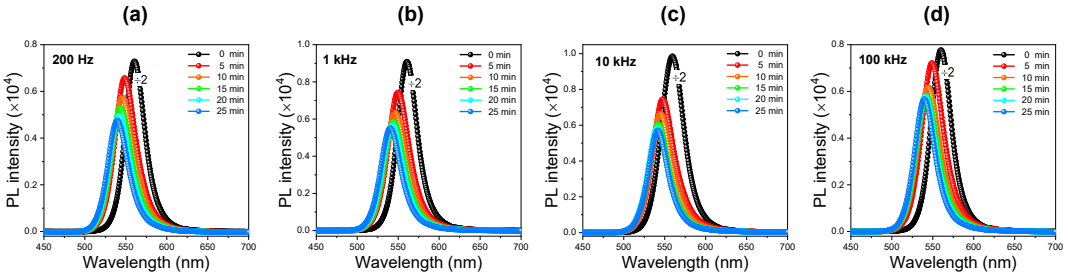

Fig. S21. PL spectra of the untreated $CsPbBr_{1.5}I_{1.5}$ QDs with different illumination times under the pulse-frequency-modulation (PFM) excitation. The duty cycle is fixed at 50%, and the repetition rates are (a) 200 Hz, (b) 1 kHz, (c) 10 kHz, and (d) 100 kHz, respectively.

In addition to the PWM approach, we also inspect the dependence of the PL stability on the repetition rate of the chopped excitation beam in the manner of the pulse-frequency-modulation (PFM) method. As detailed in the Experimental Section, the repetition rate can be finely tuned by varying the rotation speed of the optical chopper. As seen in Fig. S21, though the repetition rate is varied by a factor of 500, the PL stability is barely changed.

S22. Evolution of PL spectra for the SBE/OA/OAm-treated $CsPbBr_{1.5}I_{1.5}$ QDs under PFM excitation

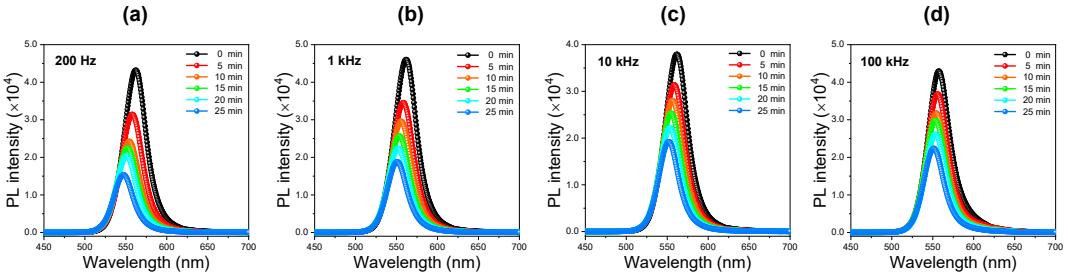

Fig. S22. PL spectra of the SBE/OA/OAm-treated $CsPbBr_{1.5}I_{1.5}$ QDs with different illumination times under the pulse-frequency-modulation (PFM) excitation. The duty cycle is fixed at 50%, and the repetition rates are (a) 200 Hz, (b) 1 kHz, (c) 10 kHz, and (d) 100 kHz, respectively.

Similar to the case shown in Fig.S21, the PL stability of the SBE/OA/OAm-treated $CsPbBr_{1.5}I_{1.5}$ QDs does not show intuitive dependence on the repetition rate as depicted in Fig. S22. Fig.S19-S22 collectively manifest that the detected PL stability is closely related to the duty cycle instead of the repetition rate of the periodically chopped excitation beam.

S23. PL intensity fluctuation of $CsPbBr_{1.5}I_{1.5}$ QDs with a reduced CW laser power

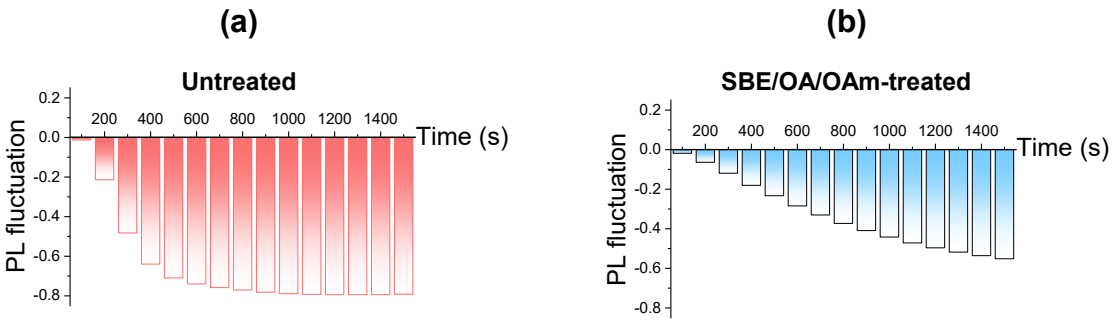

Fig. S23. PL intensity fluctuation for the (a) untreated and (b) SBE/OA/OAm treated QDs under 25-min CW excitation while the excitation power is reduced to ~15% of the original value.

The PWM approach has exhibited effectiveness in achieving long-term, stable PL from the SBE/OA/OAm-treated $CsPbBr_{1.5}I_{1.5}$ QDs solution, however, the excitation power is actually reduced compared with the CW excitation approach. For example, when working at a duty cycle of ~15% for PWM where the laser output is still fixed at 400 mW, the excitation power is reduced to 60 mW. Here we show in Fig. S23 that the decline of PL intensity upon 25-min excitation is severe for both untreated and SBE/OA/OAm-treated $CsPbBr_{1.5}I_{1.5}$ QDs solution. This implies that the enhanced PL stability in the manner of PWM excitation cannot be attributed to the weaker excitation power but to the judiciously regulated ON/OFF ratio as detailed in the manuscript.

REFERENCES

1. X. Wang, Z. Bao, Y.-C. Chang and R.-S. Liu, *ACS Energy Lett.*, 2020, **5**, 3374-3396.
2. S. Huang, Z. Li, B. Wang, N. Zhu, C. Zhang, L. Kong, Q. Zhang, A. Shan and L. Li, *ACS Appl. Mater. Interfaces*, 2017, **9**, 7249-7258.
3. H. Li, H. Lin, D. Ouyang, C. Yao, C. Li, J. Sun, Y. Song, Y. Wang, Y. Yan, Y. Wang, Q. Dong and W. C. H. Choy, *Adv. Mater.*, 2021, **33**, e2008820.
4. S. Tian, X. Zhou, C. Bi, X. Sun, M. Zhang, S. Yang and J. Tian, *Adv. Optical Mater.*, 2022, **10,** 2200751.
5. H. C. Wang, Z. Bao, H. Y. Tsai, A. C. Tang and R. S. Liu, *Small*, 2017, **14,** 1702433.
6. Y. Su, X. Chen, W. Ji, Q. Zeng, Z. Ren, Z. Su and L. Liu, *ACS Appl. Mater. Interfaces*, 2017, **9**, 33020-33028.
7. J. Zhang, T. Zhang, Z. Ma, F. Yuan, X. Zhou, H. Wang, Z. Liu, J. Qing, H. Chen, X. Li, S. Su, J. Xie, Z. Shi, L. Hou and C. Shan, *Adv. Mater.*, 2023, **35**, e2209002.
8. S. Liu, Z. Guo, X. Wu, X. Liu, Z. Huang, L. Li, J. Zhang, H. Zhou, L. D. Sun and C. H. Yan, *Adv. Mater.*, 2022, **35,** 2208078.